WELDING RESEARCH

SUPPLEMENT TO THE *WELDING JOURNAL*, JANUARY 1987

Sponsored by the American Welding Society and the Welding Research Council

An Examination of Nugget Development during Spot Welding, Using Both Experimental and Analytical Techniques

Nugget development during resistance spot welding has been studied both analytically, with a one-dimensional thermal model, and experimentally, using metallographic techniques

BY J. E. GOULD

ABSTRACT. Nugget development during spot welding has been studied using both experimental and analytical techniques. Experimentally, three gauges of an AISI 1008 steel (nominally 0.5 mm, 1 mm, and 1.5 mm/0.02, 0.04, and 0.06 in.) were studied. Current range curves, from no weld to expulsion, were generated for each of these steels at a variety of welding times. Weld times ranged for 3–20 weld cycles, the particular range of weld times used depending on the gauge of the steel. Sample welds made at each set of welding conditions (welding time and welding current) were sectioned and polished metallographically. Weld thicknesses were then measured and compared with the analytical results also generated in this work. Analytically, a numerical thermal model for the spot welding process was developed. The model is a one-dimensional finite difference formulation which takes into account all the following: melting, temperature-dependent thermal properties, electrode geometry, contact resistances, and effective heat transfer in the liquid. This model was used to predict nugget thicknesses as a function of welding conditions. A comparison of the experimental and analytical results showed them to be qualitatively consistent. Nugget growth as a function of welding variables (either welding time or welding current) could be characterized by four stages: incubation, rapid growth, steadily decreasing growth rate (shoulder), and expulsion. Quantitatively, however, there were significant deviations between the experimental and analytical results. In the heavier gauge steels, the model predicts nugget sizes significantly larger than those observed experimentally. In the light gauges, the model predicts nugget sizes significantly smaller than those observed experimentally. In the former case, the error is believed due to the model's inability to account for axial heat flow into the sheet. In the latter case, the error is attributed to inadequate data on the dependence of contact resistance on temperature.

KEY WORDS

Resistance Spot Weld
Nugget Development
Thermal Modelling
Thermal Cycles
AISI 1008 Steel
Numerical Modelling
Contact Resistance
Dynamic Resistance

Introduction

The purpose of most spot weld qualification procedures (Refs. 1, 2) is to insure that, for a given steel, a weld nugget of adequate size can be achieved. Traditionally, nugget sizes have been estimated from various destructive tests, such as peel testing or chisel testing. More recently, ultrasonics (Ref. 3) and dynamic resistivity profiles (Refs. 4–6) have been

J. E. GOULD is a Senior Research Engineer with the Edison Welding Institute, Columbus, Ohio.

Table 1—Chemical Analysis of AISI 1008 Steel

C	Mn	P	S	Si	Al	N	Fe
0.08	0.32	0.009	0.018	0.024	0.046	0.007	bal.

Table 2—As-Welded Thicknesses of Steel Used in this Study

Aim thickness	0.51 mm	1.02 mm	1.52 mm
Actual thickness	0.51 mm	1.09 mm	1.52 mm

Table 3—Welding Conditions Used in this Study

Welding Conditions	Sheet Thickness		
	0.51 mm	1.09 mm	1.52 mm
Electrode diameter	4.8 mm	6.1 mm	7.6 mm
Electrode taper	45 deg	45 deg	30 deg
Welding force	1690 nt	3020 nt	4670 nt
Welding time (range)	3–15 cyc	6–15 cyc	6–20 cyc
Welding current (range)	6–11 KA	8–13 KA	10–20 KA

used to estimate nugget sizes. Rarely, however, has the nugget size been directly and systematically correlated with the various welding variables. Analytically, attempts have been made to understand the relationships between weld development and welding variables through various thermal models (Refs. 7–14). These models are of varying degrees of sophistication, but have been of only limited use in understanding nugget development because of two points:

1. The models are process control oriented. As such, application of these models to the various metallurgical changes occurring in the steel during welding has largely been ignored.

2. Little experimental verification has been done to test these models. Little systematic work has been done to experimentally characterize the temperature cycles in these welds. As such, the results from such models have not been verified.

This work has been initiated to address some of these problems. Basically, weld nugget development was studied as a function of three variables: the welding current, the welding time, and the thickness of the sheets being welded. Nugget development was studied empirically using optical microscopy techniques. In addition, a one-dimensional heat transfer model describing the spot welding process was also developed.

The model was formulated to include the effects of: melting, temperature-dependent thermal and electrical properties of steel, heat transfer in the liquid, and contact resistances. The model was correlated with the microstructural observations, and then used to understand the influence of various factors on nugget development.

Background

Some measure of how weld nuggets develop is implicit in most automotive companies' spot weld qualification procedures (Refs. 1, 2). Generally, these qualification procedures specify measuring the size of the weld nugget as a function of one or more welding variables. The independent variable(s) used varies from specification to specification. Ford uses current as the only variable, while Fisher Body uses both welding current and welding time. The method, however, by which the nugget size is measured is always the same: destructive peel testing. Peel testing, though simple, has two inherent drawbacks:

1. The diameter rather than the thickness of the nugget is measured. Most of the heat flow during spot welding is normal to the sheet into the welding electrodes. As such, nugget development is controlled by the growth rate in this direction (thickening). Obviously, this penetration cannot be measured by peel testing.

2. The true nugget diameter is often not actually measured. During peel testing, the weld rarely fails exactly at the edge of the nugget. Usually, the weld either fails in the heat-affected zone or through a portion of the nugget. As such, accurate nugget diameters are rarely measured from peel test specimens.

More recently, dynamic resistivity profiles have been used to study nugget development (Refs. 4–6). This technique, however, has generally been applied to spot welding feedback control systems rather than understanding how nuggets develop. In addition, the measured resistivity is a function of a number of material changes other than just the nugget thickness, and as such is difficult to interpret.

Numerous authors have attempted to characterize the thermal cycles which occur during spot welding. The earliest works attempted to infer cooling rates from local hardness values (Ref. 15). Much work has also been done attempting to predict spot weld thermal cycles using closed form analytical techniques (Refs. 7–9). In order to apply these techniques, however, assumptions must be made which vastly oversimplify the spot welding process. As such, these models have been used only for a general understanding of the process.

Several authors have attempted to model the spot welding process using numerical techniques (Refs. 10–14). Greenwood (Ref. 10) developed a three-dimensional axisymmetric model which assumes: no contact resistances, constant material properties, and heat transfer into the electrode proportional to the temperature at the electrode-sheet interface.

He later correlated this model metallographically by examining welds made on single pieces of steel (no faying surfaces). His results demonstrated the importance of the various contact resistances to nugget development. Rice and Funk (Ref. 12) later developed a one-dimensional model for the spot welding of composite materials used in semiconductor fabrication. Their model accounts for: temperature-dependent material properties, joule heating, contact resistances, and thermal resistances at the contact surfaces.

This model does not, however, include any provision for melting. Houchens, *et al.* (Ref. 13), developed a similar one-dimensional model. Their work considered the effects of: melting, temperature-dependent thermal and electrical properties, and joule heating. However, the effects of the various contact resistances were not considered.

A very elaborate model dealing with both the thermal and mechanical aspects of spot welding has been developed by Nied (Ref. 14). This is a finite element formulation, in which the predicted temperature changes are used to calculate any deformation of the electrodes or sheet. The resulting solution allows prediction of the mechanical response of the weld, as well as the thermal response. The model is a three-dimensional, axisymmetric formulation, accounting for the following: temperature-dependent thermal properties, melting, and joule heating.

Again, the effects of the various contact resistances were not considered. Largely, however, the results from this analysis were applied toward understanding deformation of the welding electrodes and sheet, and growth of the weld nugget was not considered.

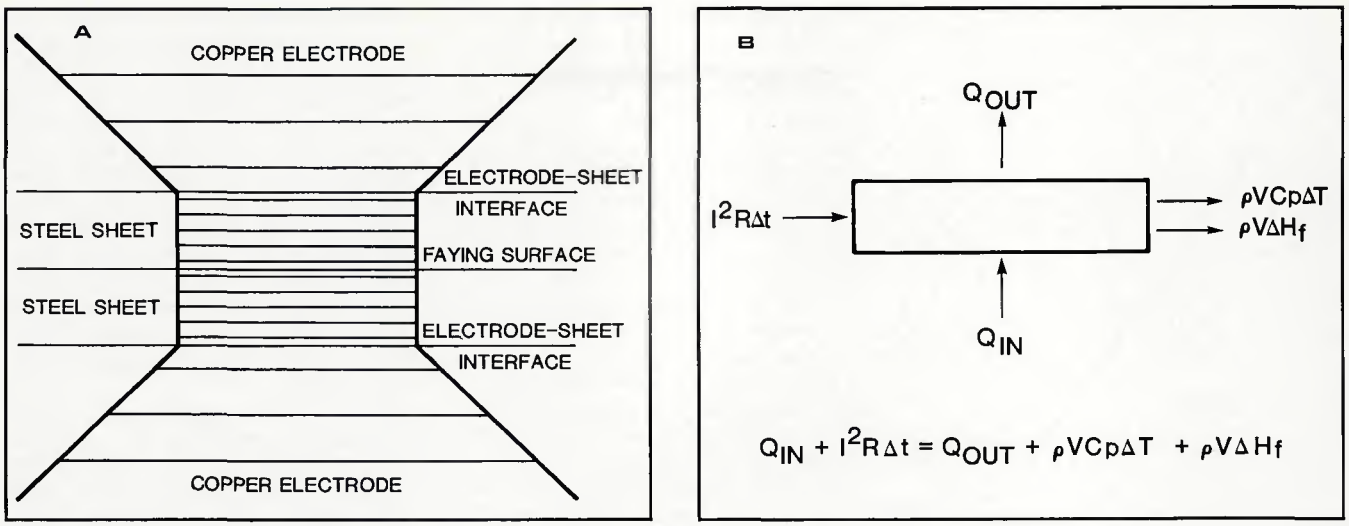

Fig. 1—Model geometry. A—Element configuration; B—Graphical description of the governing equation

Experimental

The material used in this study was an AISI 1008 steel, the exact composition given in Table 1. The material was originally supplied by the Inland Steel Indiana Harbor Works as 2.5-mm (0.1-in.) hot-rolled sheet. The material was then cold rolled to the required gauges, followed by a simulated batch anneal at 700°C (1292°F) for 10 h. The aim and final gauges of the steel are given in Table 2.

Welding was done on a Sciaky press-type 100-kVA single-phase resistance welding machine. The welding force and welding electrodes were selected as a function of gauge, based on the Ford welding specification 13-4 (Ref. 1). Additional welding times were then chosen to cover a range significantly above and below the value specified by Ford. For each welding time, welds were made at increasing current levels ranging from no weld to expulsion. Exact welding conditions are given in Table 3. All welds were subsequently sectioned through the nugget normal to the plane of the sheet, then mounted in bakelite for metallographic examination. Samples were mechanically polished and etched in a saturated solution of picric acid in water. This etching solution proved very effective in revealing the weld nugget solidification structure. Samples were characterized with a Zeiss Ultrashot metallograph, and nugget measurements were made from the resulting micrographs.

Modelling

The thermal model developed in this work is a one-dimensional, finite difference solution, mathematically similar to those developed by other workers (Refs. 12, 13). The model was designed to account for all the following aspects of the spot welding process: electrode geometry (truncated cone), temperature-dependent thermal and electrical properties, joule heating, melting, effective heat transfer in the liquid, and contact resistances.

The major innovations of this model have been in the treatment of effective heat transfer in the molten pool, and the inclusion of the various contact resistances. The major failing of the model has been its inherent inability to account for radial heat losses from the weld area to the surrounding sheet.

The element configuration used in this model is shown in Fig. 1A. The elements are platelike, and their geometry can be completely described by: the element thickness, the "weld side" diameter, and the "chill side" diameter. Elements of different thicknesses are used for the steel sheet and copper electrode in accordance with their respective thermal diffusivities. As copper has a much larger thermal diffusivity than steel, larger elements can be used (for a given time increment) without the model becoming unstable. The electrode elements used different diameters on the "weld side" and on the "chill side." This was done to account for different tapers on the truncated cone electrodes. The steel elements had both "weld side" and "chill side" diameters equal to the electrode face diameter.

A graphical description of the governing equation used in this model is shown in Fig. 1B. Basically, an energy balance is done for each element in the configuration. Energy is introduced to the element in two ways: by internal (joule) heating, and by conduction. This, in turn, is balanced by accommodating the heat internally (by an increase in temperature or melting) and by heat loss through conduction.

Heat flow in the model is, as has already been stated, one-dimensional. Heat is assumed to be generated within the weld, and conducted out through the copper electrodes. Symmetry is assumed, so the computation is done on only half the weld configuration. The boundary conditions used in this computation are as follows:

1. At zero time, the temperature is uniform at the cooling water temperature (assumed to be 25°C/77°F).
2. The electrode temperature at a distance of the electrode face diameter back from the electrode-sheet interface is assumed to remain constant at the cooling water temperature (25°C).
3. It is assumed that no heat flow occurs across the faying surface (symmetry).

The model also considers the temperature dependence of the thermal properties of steel. The actual material data used with this model is for AISI 1010 steel, and was supplied by the General Motors Technical Center (Ref. 16).

The effects of melting, both in terms of the heat required to melt and heat transfer in the liquid, are considered. With respect to the heat of melting (fusion), the steel was assumed to behave as pure iron, melting or solidifying at exactly 1527°C (2781°F). The heat of fusion was assumed to be the same as that of pure iron. Heat transfer in the liquid was considered by using an effective heat transfer coefficient. A value for the effective heat transfer coefficient of the molten pool was taken from the work of Kou (Ref. 17). Examining GTA welds on mild steel, he empirically evaluated this coefficient as about seven times the room temperature thermal conductivity of the solid.

This model also includes the effects of the various contact resistances. The electrode-sheet contact resistance was assumed to be invariant during the welding operation and was given a value of 20

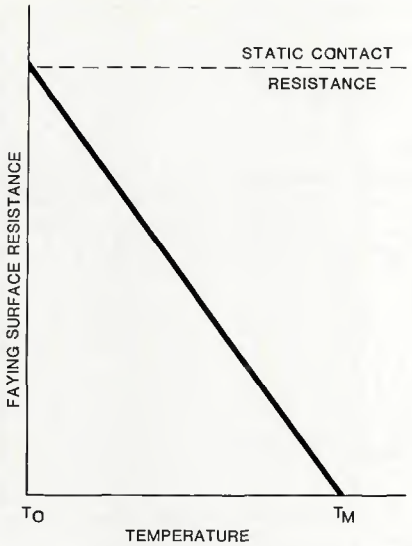

Fig. 2—Graphical description of the assumed relationship between the faying surface resistance and temperature

micro-ohms, based on the work of Savage, *et al.* (Ref. 18). The faying surface resistance, however, is assumed to be a function of temperature. This is based on the work of Dickinson (Refs. 4, 5). In lieu of any data on this dependence, it is assumed that the faying surface contact resistance varies as a linear function of temperature. This dependence is detailed graphically in Fig. 2. The endpoints for this extrapolation are:

1. The static contact resistance at room temperature. This quantity is easily measured experimentally.

2. Zero resistance at the melting point. This is clearly true, as at the melting point the faying surface resistance disappears into the molten pool.

Above the melting point, the total resistance of the weld is a function only of the electrode-sheet contact resistances, and the bulk resistivities of the liquid and solid.

Results

Micrographs showing weld nuggets as a function of each of the experimental variables are shown in Figs. 3 to 5. The etching technique employed clearly reveals the nuggets. Figure 3 details nugget development as a function of welding current for a 1.09-mm (0.04-in.) thick sheet, using a 15-cycle weld time. Qualitatively, nugget development (as a function of welding current) went through several stages. Initially, no nugget is observed (up to a current level of about 8000 A). Between 8000 and 9000 A, nugget growth is extremely rapid. Finally, between 9000 A and expulsion (10,500 A), the rate of nugget growth dramatically decreases.

Figure 4 details nugget development as a function of weld time for a 1.09-mm thick sheet using a current level of 10,000 A. Nugget growth as a function of welding time is qualitatively similar to nugget growth as a function of current. Initially, there is some incubation period. In this case, no nugget is observed up to 6 weld cycles. This is followed by a region of very rapid nugget growth, here from about 6 to 9 weld cycles. The rate of nugget growth is then observed to slow dramatically, often approaching a steady

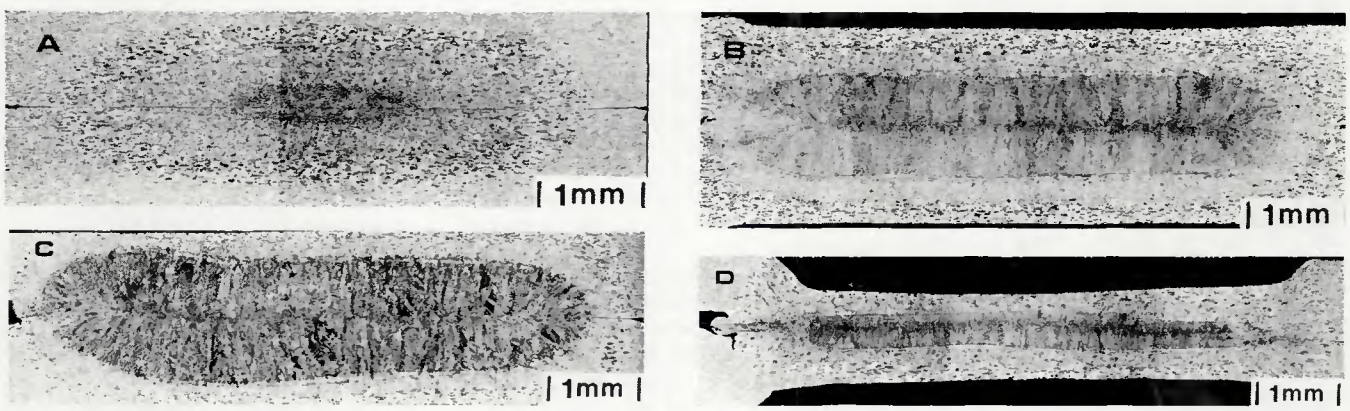

Fig. 3—Micrographs showing nugget development in a 1.09-mm sheet as a function of welding current. Welding time: 15 cycles. A—8000 A; B—9100 A; C—10,400 A; D—11,000 A

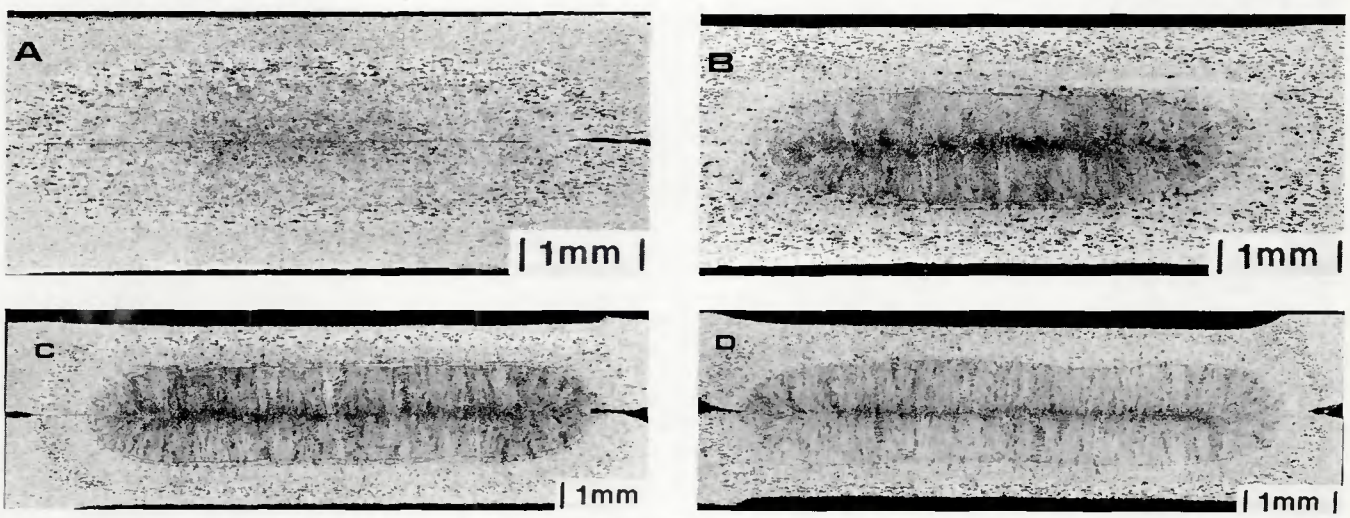

Fig. 4—Micrographs showing nugget development in a 1.09-mm sheet as a function of welding time. Welding current: 10,000 A. A—6 weld cycles; B—9 weld cycles; C—12 weld cycles; D—15 weld cycles

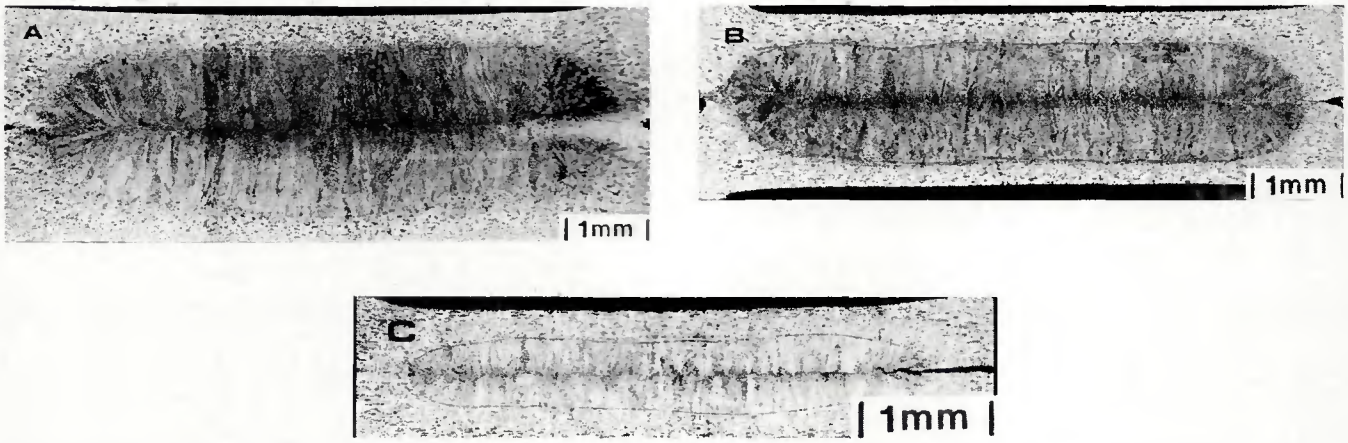

Fig. 5—Weld nugget size as a function of gauge. A—1.52-mm sheet, 14 weld cycles, 14,200 A; B—1.09-mm sheet, 12 weld cycles, 10,900 A; C—0.51-mm sheet, 9 weld cycles, 8100 A

state nugget size. Here, only small changes in nugget size were observed from 9 to 15 weld cycles, where 15 weld cycles was the upper end of the testing range.

A major qualitative difference between nugget development as a function of these two welding variables is the range over which nuggets can be formed. For the 1.09-mm sheet, the current range was only about 3000 A, or about 30% of the range from zero to expulsion. With respect to welding time, however, the range was something greater than 9 welding cycles, or greater than 60% of the range from zero to expulsion.

Figure 5 shows the effect of varying the sheet thickness. The dependence of the nugget size on sheet thickness is obscured somewhat, as many of the welding parameters (*e.g.*, welding force and electrode face diameter) are also functions of gauge. For comparative purposes, however, the welds shown in these micrographs were all made near the expulsion limit. This way, the features of fully developed nuggets can be compared. Three trends in nugget development with respect to gauge can be seen from these micrographs:

1. The nugget volume increases with gauge.
2. The degree of penetration prior to expulsion decreases with increasing gauge.
3. The aspect ratio of the fully developed nugget decreases with increasing gauge.

On the first point, larger nuggets are, of course, desirable in heavier gauge sheet, to maintain structural integrity. However, larger nuggets require larger electrodes, greater welding currents, longer welding times, and heavier welding forces. This is reflected in the various companies' spot welding procedures.

A major portion of this work concerned correlating the results from the thermal model with the experimental observations. Specifically, the model was used to predict the thickness of nuggets as a function of each of the experimental variables. Measurements of the nugget thickness were taken from micrographs such as those shown in Figs. 3 to 5.

Plots representing nugget size as a function of welding current are shown in Figs. 6 to 8. Results from both the thermal modelling and optical micrographs are included. Figure 6 shows the results for the 1.52-mm (0.06-in.) sheet welded at 6 and 20 cycle weld times. Qualitatively, both the model predictions and the nugget measurements demonstrate what was observed in the optical micrographs. That is, some initial current level must be achieved to produce any melting, and above this the nugget size increases rapidly with increasing current level. In this gauge of sheet, however, there is clearly a discrepancy between model prediction and experimental results. The model consistently predicts a nugget thickness vs. current curve similar to, but to the left of,

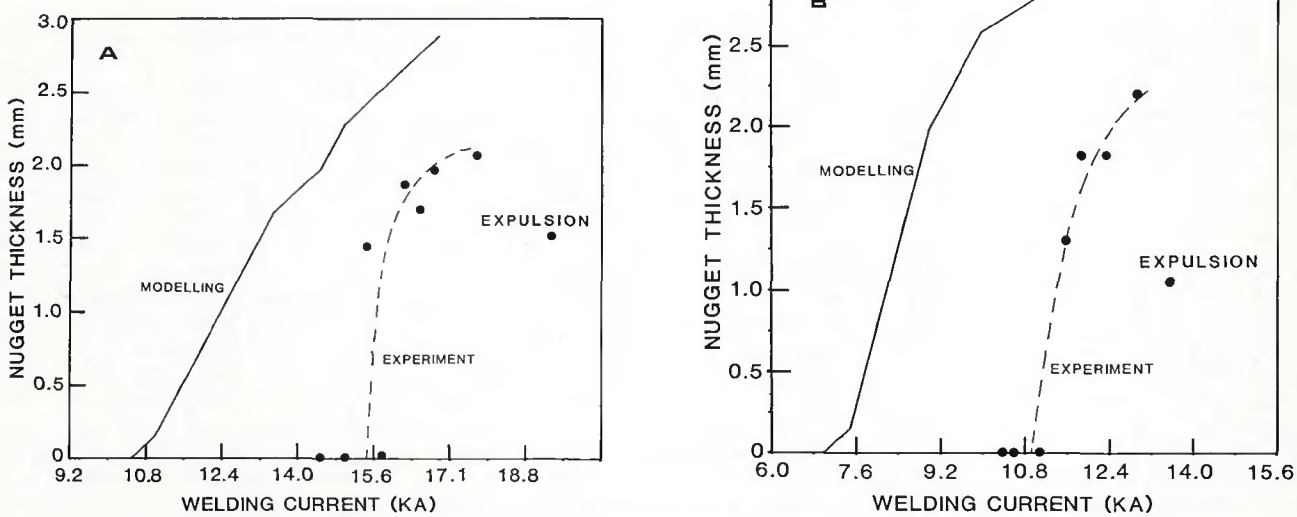

Fig. 6—Nugget size vs. current in a 1.52-mm sheet, comparison between model and experiment. A—6 weld cycles; B—20 weld cycles

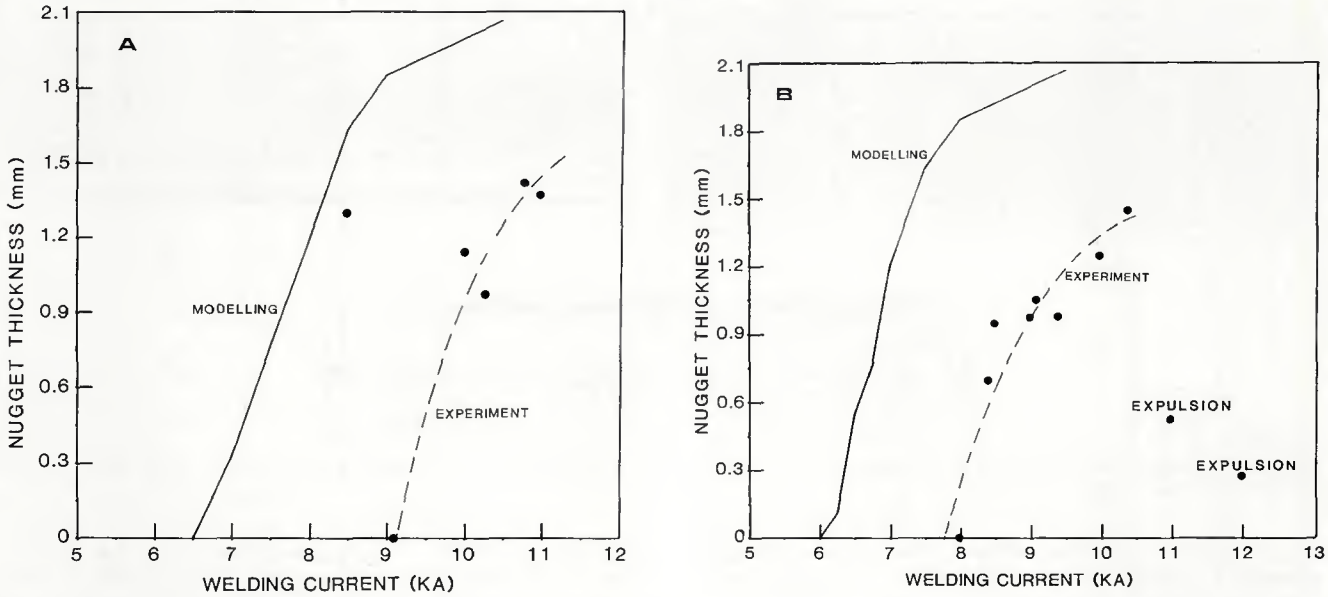

Fig. 7—Nugget size vs. current in a 1.09-mm sheet, comparison between model and experiment. A—9 weld cycles; B—15 weld cycles

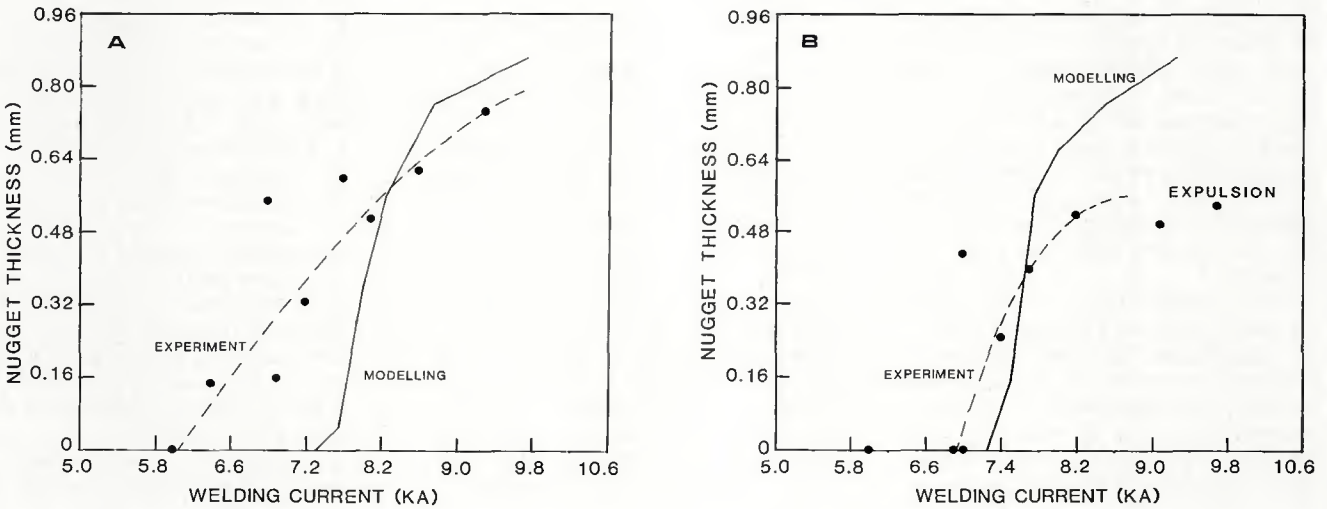

Fig. 8—Nugget size vs. current in a 0.51-mm sheet, comparison between model and experiment. A—6 weld cycles; B—12 weld cycles

the experimental data. This observation has been made previously by other authors of similar one-dimensional models (Ref. 19), and has been attributed to radial heat loss to the surrounding sheet.

Figure 7 shows some sample results for the 1.09-mm sheet welded at 9 and 15 weld cycles. The results here are similar to those for the 1.52-mm sheet. Again, the predicted nugget thickness vs. welding current curve is to the left of the experimental data, undoubtedly for the same reasons described above.

Figure 8 shows the same results for the 0.51-mm (0.02-in.) sheet welded at 6 and 12 cycle weld times. For this gauge of sheet, the model has done a significantly better job of predicting the experimental results. Apparently, for the lighter gauges of sheet, radial heat loss into the surrounding material is considerably less important than for the heavier gauges. At the upper end of the current range, the predicted nugget thickness vs. current curve agrees well with the experimental results. However, at the lower end of the current range, the predicted curve actually lies to the right of the experimental results. This indicates that heat generation during the early stages of nugget development has been underestimated.

Plots showing nugget size as a function of welding time are given in Fig. 9. Figures 9A to 9C show sample nugget thickness vs. welding time curves for each gauge of sheet for some nominal welding current. Again, both model predictions and experimental results are given in each plot. Figure 9A gives the results for the 1.52-mm sheet. Consistent with the nugget thickness vs. current results for this gauge of sheet, the predicted curve lies up and to the left of the experimental results. This again is due to radial heat losses to the surrounding sheet. The model does predict, consistent with the experimental results, an extremely large weld time "window" between initial melting and expulsion. Figure 9B represents the nugget thickness vs. welding time results for the 1.09-mm sheet welded at 10,000 A. Again, agreement between model and experiment is similar to that for the 1.52-mm sheet, for similar reasons. As with the heavier gauge sheet, a very wide welding time "window" is both predicted from the model and observed experimentally. Figure 9C shows the nugget thickness vs. welding time results for the 0.51-mm

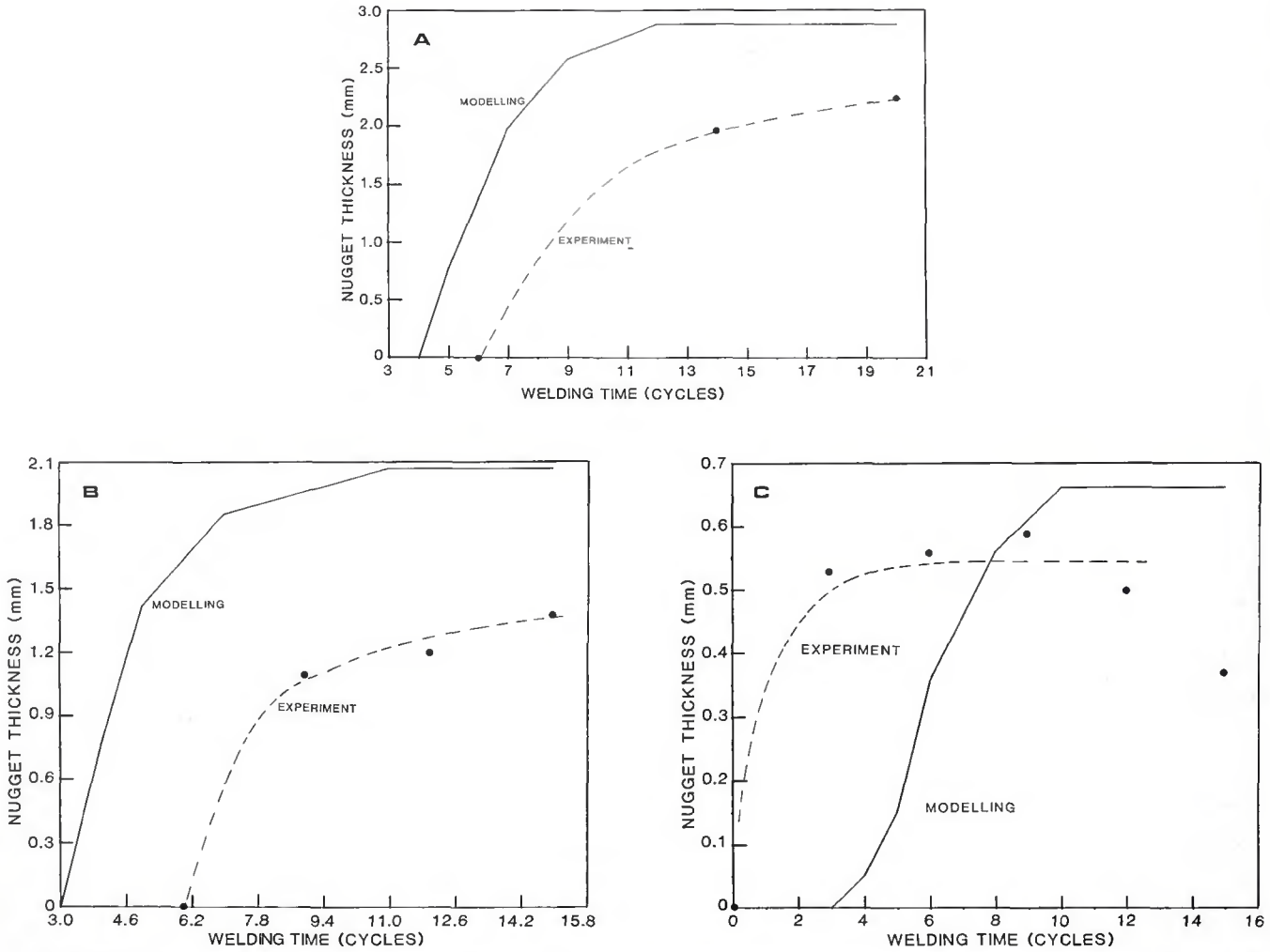

Fig. 9—Nugget size vs. welding time for the three gauges of sheet, comparison between model and experiment. A—1.52-mm sheet welded at 13,000 A; B—1.09-mm sheet welded at 10,000 A; C—0.51-mm sheet welded at 8000 A

sheet. Consistent with the nugget thickness vs. current results, the model correlates well with the experiment when the nuggets are fully developed, and less well at shorter welding times. This again (as with the nugget thickness vs. current curves) suggests that heat generation during the early stages of nugget development is being underestimated. As with the two heavier gauge steels, a very wide welding time window is both predicted from the model and observed experimentally.

The thermal model can be used, in a semiquantitative way, to examine the thermal response of spot welds. From a metallurgical standpoint, the temperature variation with respect to both time and position in the weld are important. Some examples of how temperature varies with position and time are shown graphically in Fig. 10. To generate this data, a sheet thickness of 1.09 mm was used with a welding current of 10,000 A.

Figure 10A shows the relationships between temperature and distance (from the faying surface) for several weld times. Early in the welding cycle, the temperature rise is concentrated at the faying surface (due to the large resistance there). With longer welding times, the temperature distribution broadens. This occurs presumably as the faying surface resistance decreases, and heat generation becomes more heavily dependent on the bulk resistivity. With the onset of melting, very different temperature distributions are observed in the liquid and solid. The thermal gradient in the liquid is very shallow, presumably due to the very large heat transfer coefficient the model has used for the pool. Thermal gradients in the solid, on the other hand, are very steep. This is due to the imposed thermal constraints of the weld pool on one side, and the chilled copper electrode on the other.

Figure 10B shows the temperature vs. time relationships for a few positions in the weld at varying distances from the faying surface. The "bumps" on these plots are due to an instability in the model associated with the melting and resolidification of discrete volume elements. The most metallurgically significant features which can be taken from these curves are the heating and cooling rates in the weld. The heating rates were very rapid throughout the weld, but decreased significantly with increasing distance from the faying surface. Cooling rates in the weld were somewhat less sensitive to position in the weld, and for these welding conditions (12 cycles welding time), reached a peak value of 5000°C/s (9032°F/s) in the austenite-to-ferrite transformation region.

Discussion

Qualitatively, nugget development as a function of the welding variables used in this study (welding current, welding time, and sheet thickness) is fairly straightforward. How nugget growth proceeds as a function of welding current and welding time is qualitatively similar, and can be described as:

1. Some incubation period before which no melting is observed.

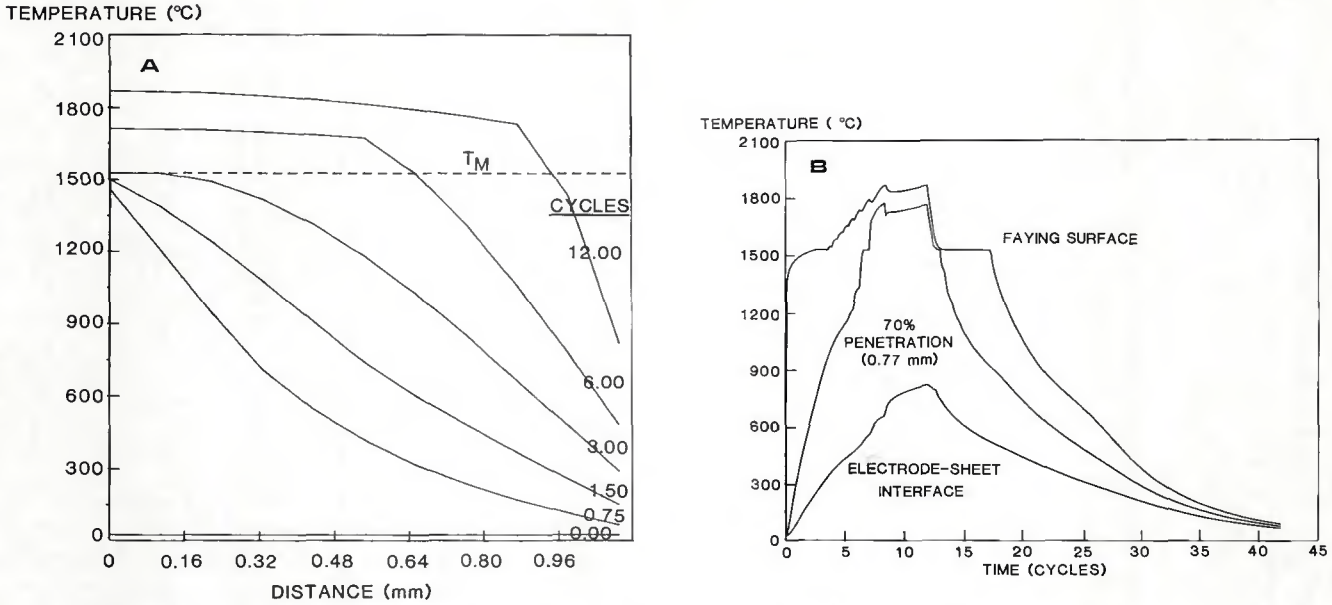

Fig. 10—Predicted thermal cycles for a 1.09-mm sheet welded at 12 weld cycles and 10,000 A. A—Temperature vs. distance; B—Temperature vs. time

2. A region of rapid nugget growth.
3. A region over which the rate of nugget growth progressively decreases.
4. Expulsion.

Differences in nugget development with respect to these two welding variables can be described as differences in the relative sizes of these regions. For example, nugget growth with respect to welding current can be characterized by a large region of incubation, small regions of rapid growth and decreasing growth, and finally expulsion. Similarly, nugget growth with respect to welding time is characterized by small regions of incubation and rapid growth, and a large region of decreasing growth. Often, this region of decreasing growth progressed to a point where the nugget was in a steady state under the applied welding current, *i.e.*, the nugget size became independent of the welding time. As a consequence, expulsion was often not observed.

As mentioned, the effect of varying the gauge was largely to vary the size of the formed nugget. This is a direct result of the larger diameter electrodes, heavier welding forces, larger welding currents, and longer welding times used with heavier gauge steels.

Some insight into the above observations can be gained by doing a simple heat flow balance on the spot welding process (this analysis is distinct from, and should not be confused with, the numerical modelling done elsewhere in this paper). This analysis assumes that the weld can be treated as a lumped thermal mass, all heat generated is conducted away by the electrodes, and the electrode-sheet contact surface remains at a constant temperature. Heat flow in the weld can be approximated by the following equation:

$$A\Delta x\,\rho C_p\,\Delta T/\Delta t = I^2R - KA\,\Delta T/\Delta x \qquad (1)$$

A is the electrode area; ρ, C_p and K are the density, heat capacity, and thermal conductivity of the steel, respectively; R is the weld resistivity; I is the welding current; Δt is the welding time; Δx is the sheet thickness; and ΔT is the total temperature rise. This expression can be rearranged to yield:

$$\Delta T = \frac{I^2R}{2K}\left[\frac{A}{\Delta x}\left[\frac{\Delta x^2}{\alpha\,\Delta t} + 1\right]\right]^{-1} \qquad (2)$$

where α is the thermal diffusivity of the steel. If ΔT is loosely equated to the nugget size, this expression, though oversimplified, can be used to interpret some of the results. Considering the welding current, ΔT is proportional to I^2. As ΔT increases as the square of the current, this suggests a relatively longer incubation time and the shorter stages of rapid growth and decreasing growth (at higher currents). As ΔT continues to rise with increasing current, expulsion is also predicted.

With respect to the welding time, the temperature rise can be described by:

$$\Delta T \propto \left[\frac{\Delta x^2}{\alpha\,\Delta t} + 1\right]^{-1} \qquad (3)$$

For short welding times, ΔT is proportional to Δt, suggesting, as is observed experimentally, small regions of incubation and rapid growth. For longer welding times, $\Delta x^2/\alpha\Delta t$ approaches zero, and ΔT approaches a constant value. A constant value of ΔT is equivalent to a steady state nugget size, and is often reached before the expulsion limit. This corresponds to the observations of a large region of decreasing growth and often no expulsion.

Interpreting this equation with respect to gauge is somewhat more difficult. However, if the expression is simplified by assuming fully developed nuggets (long weld times), ΔT is proportional to $(A/\Delta x)^{-1}$ (A is a function of Δx in any of the automotive welding schedules) (Refs. 1, 2). This shows the importance of the electrode area to sheet thickness ratio. As $A/\Delta x$ increases, it becomes increasingly difficult for the nugget to develop. This, of course, is because heat is more easily conducted away from the weld.

As mentioned, a one-dimensional finite difference model of the spot welding process has also been developed. This model has been used to gain a more quantitative understanding of nugget development. Results from this model, as well as comparison with experimental data, are shown in Figs. 6 to 9. These figures compare predicted nugget growth with measured nugget sizes as a function of welding current and welding time. Generally, the model predicts the proper shape of the curve, and gives the various regions of nugget development in the proper proportions. However, the predicted curves are usually displaced from the measured data. These discrepancies have been attributed to one of two inadequacies in the model: radial conduction in the sheet and improper characterization of the faying surface resistance. These problems are discussed below.

Radial Heat Conduction in the Sheet

The finite difference heat flow model

presented here is one-dimensional. It cannot account for heat losses into the surrounding sheet. When this type of heat loss is significant, the model overestimates the nugget size. Examples of this are seen in Figs. 6 and 7, and in Figs. 9A and 9B. Figures 8 and 9C, however, do not show this trend. Apparently, conduction into the sheet was limited for this weld configuration. To estimate the importance of heat loss to the surrounding sheet, another simple heat flow analysis can be done. Basically, one can coarsely approximate heat flow into the electrodes ($\dot{q}_e$) and surrounding sheet ($\dot{q}_s$):

$$\dot{q}_e = -KA\,\Delta T/\Delta x \qquad (4)$$

and

$$\dot{q}_s = -K\,(\pi d\,\Delta x)\,\Delta T/\,(d/2) \qquad (5)$$

where d is the electrode diameter. The first equation assumes heat to be conducted through the electrode face area over a distance of the sheet thickness (alternatively, that the electrode sheet interface remains at a constant temperature). The second equation assumes heat to be conducted through an area equal to the circumference of the electrode tip times the sheet thickness, over a distance of the electrode radius. The ratio of heat lost due to radial conduction in the sheet to heat lost through the electrodes can be approximated as $\dot{q}_s/\dot{q}_e$, or:

$$\frac{\dot{q}_s}{\dot{q}_e} = 8(\Delta x/d)^2 \qquad (6)$$

Alternately, the fraction of heat lost through radial conduction can be expressed as:

$$f_s = \frac{\dot{q}_s}{\dot{q}_s + \dot{q}_e} = \frac{8(\Delta x/d)^2}{8(\Delta x/d)^2 + 1} \qquad (7)$$

With either expression, as $(\Delta x^2/d^2) \rightarrow 0$, heat flow approaches the one-dimensional condition. Larger values of $\Delta x^2/d^2$ indicate an increasing importance of radial heat conduction in the sheet. Values of $\Delta x^2/d^2$ and f_s for the three gauges of sheet are shown in Table 4. For the gauges of sheet studied, $\Delta x^2/d^2$ varies by a factor of 4. This is consistent with the observation of significant radial heat loss in the 1.52-mm sheet, and little radial heat loss in the 0.51-mm sheet.

Proper Characterization of the Faying Surface Resistance

The faying surface resistance generally plays a large role in nugget development. This is because the faying surface is usually the highest resistive component of the welding circuit, and as such, is responsible for the greatest local heat generation. Resistivity measurements done at Inland and elsewhere (Ref. 20) have shown the static faying surface resistance is 100 to 1000 times the total resistance of a developed nugget. In addition, the faying surface also varies considerably with temperature and pressure (Refs. 4, 18). Very little quantitative work has been done, however, to characterize these resistances (especially as a function of temperature). Still, it was desired to include the (dynamic) faying surface resistance in the model. So, in the absence of any data, the author assumed that the faying surface would decrease linearly with increasing temperature.

The endpoints for this approximation were the static value (at 25°C) and zero (at the melting point). Unfortunately, this assumption has broken down. This is most clearly seen in the results from the 0.51-mm sheet. Here, it is obvious that during the early stages of nugget formation the model is unable to generate sufficient heat to predict the experimentally observed results. As such, the predicted nugget sizes are generally less than those observed experimentally. Clearly, better fit between model and experiment awaits a better characterization of the faying surface resistance.

Subject to some noticeable limitations, the model has been shown to approximate nugget growth during spot welding. This fact lends credibility to the thermal cycles the model predicts. These thermal cycles, although subject to the types of error discussed above, provide considerable insight into both how heat is generated in spot welds and the severity of the thermal cycles. As such, the remainder of this section will discuss these thermal cycles and their effects on weld structural development. Figure 10 shows predicted thermal cycle results for a 1.09-mm sheet welded at 12 weld cycles and 10,000 A.

Figure 10A shows the temperature distribution in the through-thickness direction of the sheet at fractional time increments in the weld cycle. The first observation which can be made from these curves is the relative influence the surface and bulk resistances play in the early stages of nugget development. This can be seen in the curves representing 0, 0.75, 1.5, and 3 weld cycles. During the earliest stages of heating (0.75 cycles), the surface resistance plays a dominant role in heat generation. Evidence for this comes from the shape of the curve. The curve is concave up, suggesting that heat is generated at the weld centerline and conducted into the rest of the weld. By 1.5 weld cycles, the bulk resistance has started to play a role. The curve now has a point of inflection, near the weld centerline (where the temperature and bulk resistivity are the highest). The curve is concave down, indicating bulk joule heating is dominant. Further away, the curve is still concave up, indicating the temperature rise is still controlled by heat conduction from the hotter regions of the weld. Finally, by 3 weld cycles the temperature at the faying surface has reached the melting temperature. At this point, the faying surface resistance has fallen to zero, and the temperature rise is completely dominated by the bulk resistive heating. Consequently, the curve is concave down.

Table 4—Gauge of Steel Studied

Gauge (mm)	$(\Delta x/d)^2$	f_s
0.51	0.011	0.083
1.09	0.032	0.203
1.52	0.040	0.242

These curves also give some insight into the relative thermal gradients developed in the liquid and solid. As might be expected, severe thermal gradients in the solid are required to constrain the nugget when it is fully developed. This is shown in the curves representing 6 and 12 weld cycles. Such extreme thermal gradients in the solid result in a highly compressed heat-affected zone. This can be seen in many of the micrographs of Figs. 3 to 5. Somewhat surprising are the very shallow thermal gradients in the liquid pool. This is undoubtedly due to the very high heat transfer coefficient used for the liquid. Concurrent with this observation, only a very small superheat (300°C/572°F in the 12 weld cycle curve) is found in the liquid pool. Such shallow thermal gradients, combined with the rapid solidification rates experienced during spot welding, should result in a cellular-dendritic solidification structure (Ref. 21), as has been observed (Ref. 22).

Figure 10B shows temperature-time profiles for several positions in the through-thickness direction of the weld. Some interesting features concerning nugget development can be noted from these curves. First is the influence of the surface resistance on the heating rate. The faying surface (x = 0) temperature reaches $0.9T_m$ within a small fraction of a cycle. After this, the heating rate tapers off, largely because the faying surface resistance falls with increasing temperature. These heating rates also decrease with increasing distance from the weld centerline. The degree of superheat can also be taken from these curves, and again the maximum value is about 300°C.

One of the most important results from the model is the ability to predict cooling rates. Such cooling rates can be taken from the curves of Fig. 10B. Characterizing these cooling rates is critical to understanding phase transformations in spot welds. These curves indicate cooling rates in the $\gamma \rightarrow \alpha$ transformation region of about 5000°C/s. The cooling rate appears to vary only slightly (20%) over the entire through thickness of the weld. Through the range of gauges used in this study, cooling rates from 2000°-

10,000°C/s (3632°-18,032°F) were observed. Phase transformations under these cooling rates are not very well understood, as they are more severe than water quenching (1000°C/s, or 1832°F/s), and less severe than splat quenching (10^5-10^6°C/s).

Conclusions

Nugget development of an AISI 1008 steel has been characterized as a function of the sheet thickness, welding current, and welding time. To aid in understanding these results, a one-dimensional thermal model for the spot welding process has also been developed. It was found that, both empirically and from the modelling results, nugget growth with respect to both welding current and welding time was qualitatively similar. Four stages of nugget growth were identified. These include:

1. An incubation period (no observable nugget).
2. A region of very rapid nugget growth.
3. A "shoulder" region, where the nugget growth rate progressively decreases.
4. Expulsion.

Differences in nugget growth behavior with respect to the welding current and welding time were described in terms of the relative sizes of each of these stages.

The effect of varying the sheet thickness is somewhat more difficult to interpret, as many of the welding variables are dependent on gauge. For example, both the welding force and electrode diameter vary with the gauge of steel welded. However, observations of fully developed nuggets indicate that nuggets in sheets of increasing thickness have progressively larger volumes, larger aspect ratios and a smaller degree of nugget penetration.

These results were semi-quantitatively related to the experimental variables by a simple one-dimensional heat flow analysis. That analysis yielded:

1. $\Delta T \propto I^2$ — This accounts for the rapid nugget growth rates in regions of rapid growth and decreasing growth, and the ease with which the expulsion limit is reached.
2. $\Delta T \propto [\Delta x^2/(\alpha \Delta t) + 1]^{-1}$ — This suggests that nugget growth is rapid at short welding times, but falls to zero at long welding times.
3. $\Delta T \propto (A/\Delta x)^{-1}$ — This shows nugget development is heavily dependent on the sheet thickness to area ratio.

As mentioned, a one-dimensional finite difference thermal model of the spot welding process was also developed. This model was used to predict nugget sizes as a function of the experimental variables, and these were compared with those measured optically. The model was very effective in predicting the shape of the nugget size vs. current and nugget size vs. welding time curves. However, the results were usually displaced to some degree. Some reasons for this displacement are:

1. Radial heat flow in the sheet — A simple heat flow analysis was done to estimate the relative rates of heat withdrawal through the electrodes and radially into the sheet. It was found that the ratio of these rates of heat withdrawal could be expressed as:

$$\frac{\dot{q}_s}{\dot{q}_e} = 8\left(\frac{\Delta x}{d}\right)^2 \qquad (8)$$

Alternatively, the fraction heat lost into the sheet compared to the total heat conducted away from the weld could be expressed as:

$$f_s = \frac{\dot{q}_s}{\dot{q}_s + \dot{q}_e} = \frac{8(\Delta x/d)^2}{8(\Delta x/d)^2 + 1} \qquad (9)$$

f_s varies from zero when the electrode diameter is large compared to the sheet thickness (one-dimensional heat flow), and to 1 when $\Delta x >> d$ (radial heat flow only). Clearly, the smaller the value of f_s, the more accurate the one-dimensional model described in this work becomes.

2. Inadequate characterization of the faying surface resistance — The faying surface resistance, and especially its dependence on temperature, is not well understood. In lieu of any data in this area, the author assumed the faying surface resistance decayed linearly (from the static value) with increasing temperature. This approximation is apparently inadequate, as borne out by the results from the 0.51-mm sheet. Similar error is undoubtedly present in the nugget growth predictions for the heavier gauge sheets, but is apparently masked by radial heat loss effects. Clearly, further refinement of the model in this area awaits better faying surface temperature data.

Finally, the model was used to describe thermal cycles in some of these welds. From the modelling results, it was possible to estimate:

1. Superheat in the weld nuggets.
2. Thermal gradients in the liquid and solid.
3. Cooling rates in the weld.

All of the above have a significant influence on weld nugget development.

Acknowledgments

The author would like to express his thanks to the Inland Steel Company, where this work was done. He would also like to thank Dr. A. G. Preban, Dr. P. H. Chang, Mr. W. Schumacher, and Mr. B. S. Levy for their helpful criticisms of the work; Drs. S. Kou and W. H. Yang for their helpful discussions; and the General Motors Technical Center for supplying the temperature-dependent material properties data. Finally, a special thanks to Mr. Neal Saboff, who carried out most of the experiments.

References

1. *Ford Laboratory Test Methods,* Schedule BA 13-4. September 26, 1980.
2. *Fisher Body Weld Lobe Procedure.* December 1983.
3. Spot welding sheet steel. AISI Technical Report, SG-936, 282-10M-RI.
4. Dickinson, D. W. 1981. *Welding in the Automotive Industry.* SG 81-5, submitted to DOT and AISI, April 1981.
5. Dickinson, D. W., Franklin, J. E., and Stanya, A. 1980. Characterization of spot welding behavior by dynamic electrical parameter monitoring. *Welding Journal* 60(6):170-s to 176-s.
6. Dickinson, D. W., and Natale, T. V. 1982. The effect of sheet surface on spot weldability. *Technological Impact of Surfaces,* April 14-15, 1981, ASM, Metals Park, Ohio.
7. Roberts, D. K., Roberts, J. E., and Wells, A. A. 1958. Fundamental resistance welding investigations. *British Welding Journal* 5(3): 117-126.
8. Archer, G. R. 1960. Calculations for temperature response in spot welds. *Welding Journal* 39(8):327-s to 330-s.
9. Myers, P. S., Uyehara, O. A., and Borman, G. L. July 1967. Fundamentals of heat flow in welding. *Welding Research Council Bulletin,* No. 123.
10. Greenwood, J. A. 1961. Temperatures in spot welding. *British Welding Journal* 8(9):316-322.
11. Bentley, K. P., Greenwood, J. A., Knowlson, P. McK., and Baker, R. G. 1963. Temperature distributions in spot welds. *British Welding Journal* 10(12):613-619.
12. Rice, W., and Funk, E. J. 1967. An analytical investigation of the temperature distributions during resistance welding. *Welding Journal* 46(4):175-s to 186-s.
13. Houchens, A. F., Page, R. E., and Yang, W. H. 1977. Numerical modelling of resistance spot welding. *Numerical Modelling of Manufacturing Processes,* presented at the Winter Meeting of ASME, November 27-December 2, 1977, pp. 117-129.
14. Nied, H. A. 1984. The finite element modelling of the resistance spot welding process. *Welding Journal* 63(4):123-s to 132-s.
15. Heuschkel, J. 1947. Some metallurgical aspects of carbon steel spot welding. *Welding Journal* 24(10):560-582.
16. General Motors Technical Center. Unpublished research.
17. Kou, S. Private communication, January 1984.
18. Savage, W. F., Nippes, E. F., and Wassel, F. A. 1978. Dynamic contact resistance of spot welds. *Welding Journal* 57(2):43-s to 50-s.
19. Yang, W. H. Private communication, October 1983.
20. Roberts, W. L. 1951. Resistance variations during spot welding. *Welding Journal* 28(11):1004-1019.
21. Felmings, M. C. 1974. *Solidification Processing,* McGraw-Hill, New York, N. Y.
22. Chang, P. H., and Gould, J. E. Unpublished research.

Detectability and Significance of Buried Tears in Welded T-Joints

Detection by UT is hindered by the characteristics of lamellar tearing

BY R. D. STOUT AND J. H. KOH

Introduction

In previous projects (Refs. 1, 2) funded by the American Iron and Steel Institute at Lehigh University, the influence of welding variables on lamellar tearing was investigated, and a study was conducted on the extent to which buried lamellar tears affected the static and fatigue properties of a welded steel that is susceptible to lamellar tearing. In a T-joint loaded cyclically in bending, the fatigue strength was lowered significantly by buried tears directly beneath the toe of the weld, even if they intercepted less than 10% of the supporting area. The toughness was also found to decrease in proportion to the extent of tearing.

As a consequence of the findings on the effects of buried lamellar tears on mechanical properties, it was decided to determine whether ultrasonic (UT) inspection methods can be relied upon to detect buried tears when they reach a size that may produce a meaningful loss of mechanical properties. The general approach was to produce lamellar tearing of various sizes in a series of T-joints, UT inspect them to determine the indications obtained by tearing, and cross-section the joints to reveal the actual extent of tears and thus the capability of the UT inspection. Several of the joints were also examined by industrial qualified inspectors.

Additional specimens were prepared covering a range of tear sizes to determine their effect on the static strength of a T-joint in tension and in bending.

Paper sponsored by the AISI Engineering Subcommittee and presented at the 67th Annual AWS Meeting, held April 14-18, 1986, in Atlanta, Ga.

R. D. STOUT and J. H. KOH are with the Department of Materials Science and Engineering, Lehigh University, Bethlehem, Pa.

Experimental Program

The cantilever-beam lamellar-tearing test shown schematically in Fig. 1 was originally developed at Lehigh to permit external loading of the weld joint under controlled tension during and after each weld pass, to determine the critical stress level required to originate and propagate lamellar tears. Subsequently, it was found possible (Ref. 2) to operate the test procedure so as to induce a limited extent of tearing short of complete failure. This was accomplished by applying a critical load to the weld joint, which was also monitored by an untuned acoustic-emission sensor attached to the cantilever. A relaxation of the load accompanied by an increased emission intensity signaled the beginning phases of tearing. Release of the load at the proper instant interrupted tearing when it had just begun or at any point short of complete failure, resulting in a partial tear that remained completely buried. Furthermore, the cantilever beam could then be sawed off close to the

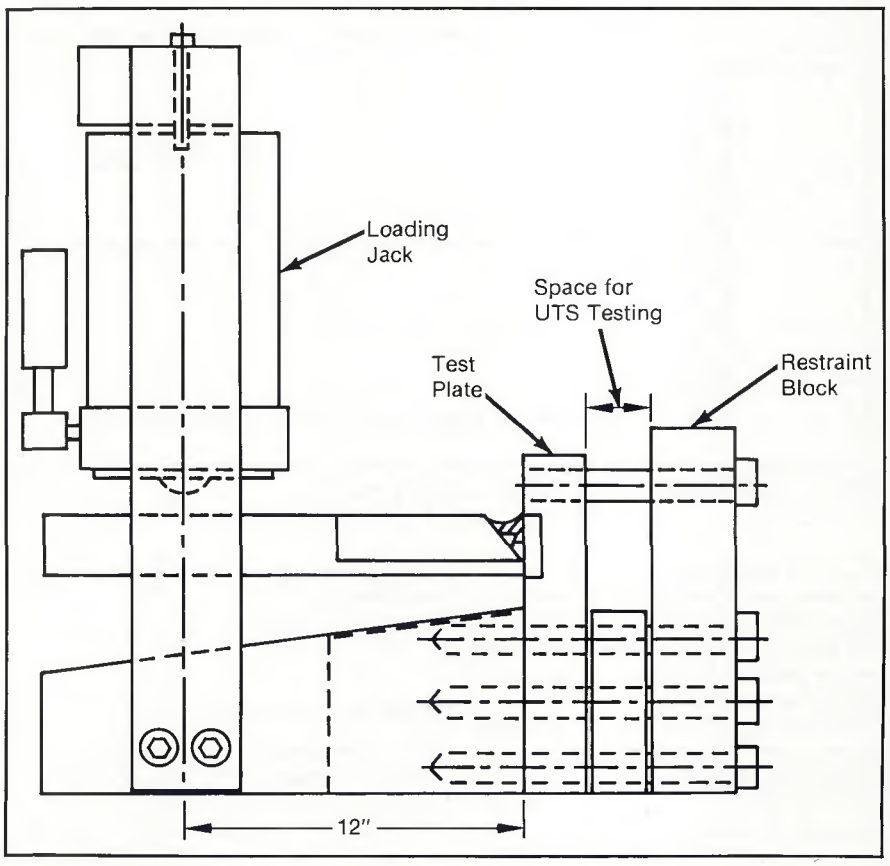

Fig. 1—Lehigh lamellar tearing fixture